






Nuclear matter and neutron star properties constrained by CREX results and astrophysical constraints: A covariance study*

Sunil Kumar¹  Vikesh Kumar²  Pankaj Kumar³  Raj Kumar^{1†}  Shashi K Dhiman^{1,4‡} 

¹Department of Physics Himachal Pradesh University, Summer-Hill, Shimla- 171005, India

²Department of Physics Sardar Patel University, Mandi- 175001, India

³Department of Applied Sciences, CGC College of Engineering, Landran, Mohali 140307, India

⁴School of Applied Sciences Himachal Pradesh Technical University, Hamirpur - 177001, India

Abstract: The ground state properties of finite, bulk matter, and neutron stars are investigated using a proposed effective interaction (HPU4) of the relativistic mean field model (RMF) that incorporates self and cross-couplings of σ , ω , and ρ mesons with nucleons. This interaction has been constructed by fitting data on binding energies and charge radii of finite nuclei, neutron skin (Δr_{np}) of ^{48}Ca nucleus, and astrophysical observations of the maximum masses of neutron stars. $\Delta r_{np} (^{48}\text{Ca}) = 0.146 \pm 0.019$ fm is achieved with soft symmetry energy ($J_0 = 27.91 \pm 1.31$ MeV) and its corresponding slope ($L_0 = 42.85 \pm 14.26$ MeV) at saturation density. An equation of state (EoS) with a composition of β -equilibrated nucleonic and leptonic matter is computed. The nuclear matter and neutron star properties are also analyzed for this interaction and agree well with the astrophysical observations, such as the NICER and GW170817 events. We also perform a statistical analysis to estimate the theoretical errors in coupling parameters and neutron star observables and to determine the correlation coefficients. We observe that the neutron skins of ^{208}Pb and ^{48}Ca are strongly correlated and exhibit a strong dependence on J_0 , L_0 and the curvature of symmetry energy (K_{sym}) as suggested from their correlations. A strong correlation of canonical mass neutron star radius, $R_{1.4}$ with ρ -meson-nucleon coupling quantified by the term $g_{\rho N}$ and mixed interaction terms $\sigma\rho_\mu\rho^\mu$ and $\sigma^2\rho_\mu\rho^\mu$ is also observed.

Keywords: relativistic mean field, equation of state, neutron star, tidal deformability, covariance analysis

DOI: 10.1088/1674-1137/adc65b **CSTR:** 32044.14.ChinesePhysicsC.49074109

I. INTRODUCTION

Neutron, strange, and hybrid stars provide unique opportunities to study dense matter and its interactions at levels comparable to terrestrial laboratories. These complicated astrophysical sources have resulted in advanced findings in nuclear and subnuclear physics, quantum chromodynamics, the general theory of relativity, and high-energy physics. Neutron stars play a significant role in physics and astronomy. Their density ranges from a few g cm^{-3} at their surface to over $10^{15} \text{ g cm}^{-3}$ in the center, with the pressure exceeding $10^{36} \text{ dyne cm}^{-2}$. The very dense core of a compact star provides an opportunity to study nuclear matter beyond saturation density. At such high densities, the composition of the matter to date cannot be known, and an equation of state (EoS) can determine the thermodynamic state of matter. To understand neutron star properties, we must know the pressure and energy density (EoS) in the high-density domain. Astro-

physical investigations exploring the mass, radius, and tidal deformability of neutron stars have revealed restrictions on EoSs. The LIGO and VIRGO collaborations [1, 2], as well as NICER mass-radius measurements [3, 4], have made significant contributions to the understanding of the dynamics of EoSs from low to high-density regimes. The Calcium Radius Experiment (CREX) has recently provided a neutron skin $\Delta r_{np} (^{48}\text{Ca}) = 0.121 \pm 0.026$ fm [5], which favors a smaller value of L . PREX-II has provided $\Delta r_{np} (^{208}\text{Pb}) = 0.283 \pm 0.071$ fm [6].

As discussed in [7–9], explaining parity-violating asymmetry across these nuclei is challenging. The origin of the Δr_{np} value reported by the CREX and Pb Radius Experiment (PREX) collaborations as thin for ^{48}Ca and thick for ^{208}Pb remains a puzzle. CREX results build on the accomplishment of PREX [6, 10], which attempted to restrict the EoS of asymmetric dense matter near ρ_0 by estimating the neutron skin of ^{208}Pb . Symmetry energy is the energy necessary to turn symmetric nuclear matter

Received 23 November 2024; Accepted 27 March 2025; Published online 28 March 2025

* Sunil Kumar is highly thankful to CSIR-UGC (Govt. of India) for providing financial assistance (NTA/ 211610029883 dated 19/04/2022) under the Junior/Senior Research Fellowship scheme

[†] E-mail: 1raj.phy@gmail.com

[‡] E-mail: 2shashi.dhiman@gmail.com

©2025 Chinese Physical Society and the Institute of High Energy Physics of the Chinese Academy of Sciences and the Institute of Modern Physics of the Chinese Academy of Sciences and IOP Publishing Ltd. All rights, including for text and data mining, AI training, and similar technologies, are reserved.

(SNM) ($N = Z$) into highly asymmetric dense matter, also known as pure neutron matter (PNM), indicating a strong relationship between finite nuclei and compact stars. Relativistic mean-field (RMF) models have become standard techniques for precisely describing finite nuclei and neutron star structures. These models remain crucial for understanding high-energy phenomena and dense nuclear matter, as they are essential to addressing the nuclear EoS in a relativistic approach [11]. The study of neutron stars exposes their complicated interior structures. Exotic matter may appear in the interior or core of a neutron star. Neutron star observables, such as maximum mass (M_{max}), radius (R), and tidal deformability (Λ), can be well characterized by the interaction between nucleons and mesons using a Lagrangian or energy density functional (EDF). This imparts an EoS, which is used to compute the observables of a neutron star.

Recent advancements in the RMF models have significantly enhanced our understanding of nuclear and neutron star properties. In recent decades, several nuclear EDF models have been employed to study finite nuclei and dense matter with diverse compositions and establish nuclear EoSs. These models include various non linear self-interactions and mixed interactions of σ , ω_μ , ρ_μ , and δ mesons and agree well with astrophysical observations. Many nuclear theories or model parameter sets, such as NL3 [12], TM1 [13], FSUGold [14], FSUGold2 [15], BigApple [16], HPU's [17], DOPs [18], OMEGs [19], DINOs [20], and HPDs [21] for the nonlinear relativistic mean field model (NL-RMF), have been widely used to study the various properties of neutron stars, such as maximum mass, radius, and tidal deformability corresponding to a canonical mass neutron star as observed from various astrophysical observations, gravitational wave events, and bulk nuclear matter parameters along with finite nuclear properties.

The contributions from σ - ω cross-couplings and self-coupling of ω mesons play important roles in varying the high-density behavior of the EoSs. The mixed interaction terms involving the ρ -meson field contribute to the isovector part of the effective Lagrangian density along with the usual linear couplings of ρ to the nucleons. The σ - ρ and ω - ρ cross-coupling terms enable us to constrain the linear density dependence of the symmetry energy and neutron-skin thickness in heavy nuclei over a wide range without affecting the other properties of finite nuclei [22].

The Effective Field Theory (EFT) requires that coupling parameters within the EDF exhibit "naturalness," meaning that these parameters should be of similar order of magnitudes (around unity) when expressed as dimensionless ratios. This naturalness condition enables a reasonable estimation of contributions to the EDF and aids in determining a suitable truncation scheme. The RMF model incorporates all possible self and mixed interaction terms for σ , ω , and ρ mesons while ensuring that adjusted

coupling parameters correspond with experimental nuclear observables [23]. Studies indicate that RMF models with terms up to order $\nu = 4$ effectively describe finite nuclei, whereas higher-order terms only marginally improve fits [24]. The primary influence on the EoS for neutron matter results from the quartic self-interaction of the ω meson, and incorporating mixed interaction terms is crucial for maintaining the naturalness of coupling parameters, as specified by the EFT [23–25]. Improvements in naturalness can be further achieved by incorporating higher-order terms involving field gradients [23].

The RMF formalism provides a computationally efficient alternative to complex nuclear many-body calculations [23] by utilizing meson-exchange interactions in a mean-field approximation, rather than direct nucleon-nucleon interactions. Conventional methods, such as Brueckner-Hartree-Fock theory, are computationally intensive and limited in their scope owing to the challenges of solving intricate many-body equations. The RMF model simplifies these interactions through phenomenological coupling constants that reflect nucleon correlations while adhering to naturalness behavior to maintain predictive accuracy. Extensions of the RMF model enhance its effectiveness in predicting properties of neutron-rich matter and neutron stars, capturing essential many-body physics without the full complexity of explicit calculation. The RMF models are based on the many-body field theory. In principle, the so-called four-, six-, higher order many-body interactions have been included naively through Dyson's equation. In non-relativistic cases, the three-body force is required even to reproduce the saturation mechanism of nuclear matter. However, it still has a large ambiguity, and such calculations encounter the problem of causality. This is also true for the chiral EFT. Therefore, we can at least insist that the relativistic calculations are suitable for describing nuclei and neutron stars compared with those calculations.

Previous studies have extensively investigated nuclear matter properties, such as the symmetry energy and maximum mass of neutron stars, but significant gaps remain in understanding how these factors collectively influence neutron star observables. Specifically, the role of the slope of symmetry energy (L) in determining neutron skin thickness and its impact on the softness or stiffness of the EoS in a high-density regime remains uncertain. While most of these studies have focused on constraining the EoS using PREX-II data, the complementary CREX results, which provide valuable insights into the neutron skin of heavy nuclei, have often been ignored. Ref. [26] investigated the implications of PREX-II on the EoS of neutron-rich matter. The study discussed in Refs. [19] incorporated the δ - N coupling and mixing terms of σ - δ mesons within the Lagrangian of the RMF model to study the combined analysis of PREX-II and CREX results. However, they were unable to simultaneously reproduce

the empirical values of Δr_{np} for ^{208}Pb and ^{48}Ca . Furthermore, as mentioned in Refs. [8, 19, 27], comprehending the results from CREX and PREX-II remains challenging, even when the mixing terms of δ - N and σ - δ mesons are included in the RMF model. In Ref. [28], effective interactions based on a relativistic EDF with density-dependent point couplings were developed to study the implications of CREX and PREX-II results on the properties of finite nuclei and nuclear matter. The data from CREX and PREX-II have been directly utilized to constrain the relativistic EDFs. However, the Δr_{np} values calculated from these EDFs do not appear to be consistent, and they indicated that no consistent conclusion from the theoretical side could be obtained when using CREX and PREX-II results. Recently, as reported in [20, 21], EDFs have been calibrated to accurately reproduce the binding energies and charge radii of spherical nuclei while accommodating the constraints set by CREX and PREX-II results. These models provide a plausible solution to the PREX-II–CREX dilemma; however, despite their consistency with the properties of finite nuclei, their large values for K_{sym} result in significant stiffening of the EoS at high densities relevant to neutron stars. This stiffening leads to larger neutron star radii and an increased tidal deformability, which is inconsistent with data from LIGO-Virgo and NICER missions.

The objective of this paper is to investigate the impact of CREX results measured at Jefferson Laboratory on the neutron skin thickness (Δr_{np}) of ^{48}Ca [5] on finite nuclear properties (binding energies and charge rms radii), neutron skin thickness of ^{208}Pb , and neutron star observables satisfying the astrophysical constraints. CREX does not directly measure Δr_{np} but instead determines the parity-violating asymmetry (A_{PV}) in elastic electron scattering, which is sensitive to the weak charge distribution and thus provides an indirect probe of the neutron density profile. By comparing the measured A_{PV} with nuclear structure models, we infer Δr_{np} . To achieve this, we construct a new set of effective interactions for the Lagrangian density of the RMF model, which includes different non-linear self and mixed interactions among isoscalar-scalar σ , isoscalar-vector ω , and isovector-vector ρ mesons up to the quartic order. In this work, the new effective interaction is searched in view of CREX results (Δr_{np} for ^{48}Ca), which are used to constrain the linear density dependence of symmetry energy and finite nuclear properties (binding energies and charge rms radii). Additionally, it is searched in the context of the prediction of maximum neutron star mass around $\approx 2M_{\odot}$ recently observed with LIGO and Virgo of the GW170817 event [29, 30] of binary neutron stars merger, the discovery of neutron stars with masses around $\approx 2M_{\odot}$ [1–4, 31–35], and the limits of dimensionless tidal deformability of a canonical neutron star as observed by the GW170817

event [1]. We also perform a statistical analysis to quantify theoretical errors in parameters and physical observables and identify correlation coefficients.

The study takes a methodical approach, with a brief outline of the RMF model's Lagrangian, equations of motion of nucleons and mesons, and EoS of infinite nuclear matter in Section II. Section III provides a detailed explanation of our findings and comments. We summarize the findings in Section IV.

II. THEORETICAL FORMALISM

The effective Lagrangian of the RMF model depicts the interactions of nucleons with σ , ω_{μ} , and ρ_{μ} mesons. The inclusion of mixed interaction terms introduces variability in the linear density dependence of the symmetry energy coefficient and neutron skin thickness of heavier nuclei. Importantly, the self-interaction of the ω_{μ} meson significantly affects the high-density behavior (soft or stiff) of EoSs and the structural properties of neutron stars. The impact of incorporating the self-interaction coupling ζ of ρ_{μ} mesons is smaller and its effect is observed to be appreciable in stars composed of PNM at high densities; the maximum masses of stars computed with β -equilibrated matter exhibit slight changes when this coupling is varied within the bounds imposed by naturalness [36]. In this paper, we have not considered the contribution from coupling ζ . The σ and ω mesons are included to consider the attractive and repulsive contributions of the nucleon-nucleon potential and are represented by an isoscalar Lorentz scalar and Lorentz vector field σ and ω_{μ} . As we propose an effective interaction for the RMF model that describes both finite nuclei and asymmetric nuclear matter, we also include the ρ meson to model the isospin dependence of the interaction. Although it does not contribute to infinite SNM, it has an important role when the isospin asymmetry is introduced, as well as for the accurate description of finite nuclei properties such as binding energies and neutron skin. It is denoted by isovector Lorentz vector ρ_{μ} .

The Lagrangian density for the RMF model with σ , ω_{μ} , and ρ_{μ} mesons and nucleons ($N = n, p$) up to the quartic order [18, 25] is

$$\begin{aligned} \mathcal{L} = & \sum_{N=n,p} \bar{\Psi}_N \left[i \gamma^{\mu} \partial_{\mu} - (M_N - g_{\sigma N} \sigma) - \left(g_{\omega} \gamma^{\mu} \omega_{\mu} + \right. \right. \\ & \left. \left. \frac{1}{2} g_{\rho} \gamma^{\mu} \tau_N \cdot \rho_{\mu} + e \gamma^{\mu} \frac{1 + \tau_{3N}}{2} A_{\mu} \right) \right] \Psi_N \\ & + \frac{1}{2} (\partial_{\mu} \sigma \partial^{\mu} \sigma - m_{\sigma}^2 \sigma^2) - \frac{\bar{\kappa}}{3!} g_{\sigma N}^3 \sigma^3 - \frac{\bar{\lambda}}{4!} g_{\sigma N}^4 \sigma^4 \end{aligned}$$

$$\begin{aligned}
& -\frac{1}{4}\omega_{\mu\nu}\omega^{\mu\nu} + \frac{1}{2}m_\omega^2\omega_\mu\omega^\mu + \frac{1}{4!}\zeta g_{\omega N}^4(\omega_\mu\omega^\mu)^2 - \frac{1}{4}\rho_{\mu\nu}\rho^{\mu\nu} \\
& + \frac{1}{2}m_\rho^2\rho_\mu\rho^\mu + \frac{1}{4!}\xi g_{\rho N}^4(\rho_\mu\rho^\mu)^2 + g_{\sigma N}g_{\omega N}^2\sigma\omega_\mu\omega^\mu \\
& \times \left(a_1 + \frac{1}{2}a_2g_{\sigma N}\sigma\right) + g_{\sigma N}g_{\rho N}^2\sigma\rho_\mu\rho^\mu \left(b_1 + \frac{1}{2}b_2g_{\sigma N}\sigma\right) \\
& + \frac{1}{2}\Lambda_v g_{\omega N}^2 g_{\rho N}^2 \omega_\mu\omega^\mu \rho_\mu\rho^\mu - \frac{1}{4}F_{\mu\nu}F^{\mu\nu} \\
& + \sum_{\ell=e,\mu} \bar{\Psi}_\ell (i\gamma^\mu \partial_\mu - M_\ell) \Psi_\ell.
\end{aligned} \quad (1)$$

Here, $F_{\mu\nu} = \partial_\mu A_\nu - \partial_\nu A_\mu$, and A is the photon field. M_N , m_σ , m_ω , and m_ρ indicate the nucleon and respective meson masses. The parameters $g_{\sigma N}$, $g_{\omega N}$, and $g_{\rho N}$ quantify the couplings that represent the interaction of nucleons with the corresponding mesons. $\bar{\kappa}$ and $\bar{\lambda}$ represent self-interactions of sigma meson, whereas ζ denotes the fourth-order self-interaction term of the omega meson. In the Lagrangian density, coupling terms such as Λ_v , (a_1, a_2) , and (b_1, b_2) represent cross interactions between $(\omega_\mu - \rho_\mu)$, $(\sigma - \omega_\mu)$, and $(\sigma - \rho_\mu)$ mesons, respectively. In Eq. (1), summation is taken over the nucleon ($N = p, n$) and leptons ($\ell = e, \mu$). In this study, only the neutron and proton have been considered for the calculation of finite nuclear matter and neutron star properties. The electromagnetic interaction is also included through the photon field A , where $F_{\mu\nu}$ is the electromagnetic field tensor.

The cubic and quartic self-interaction terms ($\bar{\kappa}$, $\bar{\lambda}$) of the σ -meson are essential in RMF models, significantly improving the nuclear matter EoS beyond the original Walecka model [37]. The introduction of these self-interactions in the Lagrangian of RMF model softens the scalar potential, leading to improved nuclear saturation properties and helping to reduce the nuclear matter incompressibility (K) to more reasonable values (200–300 MeV) and providing a density-dependent effective mass for nucleons [38, 39]. The absence of these couplings predicts an excessively stiff EoS with an unrealistically high value of $K \approx 500$ MeV as in the Walecka model [37]. The ω meson self-interaction term ζ plays a very important role in determining the soft and stiff behavior of the EoS at high densities without affecting the bulk nuclear matter properties. The neutron star mass has a strong dependence on the coupling ζ [16, 25, 36, 40]. The σ - ω mixed interactions improve the description of isoscalar nuclear interactions, whereas the σ - ρ terms are critical for accurately modeling isovector interactions such as symmetry energy. The σ - ρ and ω - ρ cross-coupling terms along with $g_{\rho N}$ account for the isovector part of the Lagrangian density and play a significant role in constraining the linear density dependence of the symmetry energy and neutron-skin thickness of finite nuclei without affecting the other properties of finite nuclei [22]. The contribution from the

mixed interaction terms of σ - ω , σ - ρ and ω - ρ mesons in the Lagrangian of the RMF model must be incorporated into the Lagrangian to accommodate the naturalness behavior of coupling parameters as imposed by the effective field theory [17, 23, 24]. Other higher-order terms, such as those involving higher powers of meson fields or more complex meson mixing, would introduce excessive parameters and lead to unphysically large or small values, violating the naturalness criterion. These selected terms enable a balance between the richness of interaction and simplicity of the model, ensuring that the theory remains predictive without introducing artificial complexities.

The equation of motion for nucleons and respective mesons can be calculated using the conventional Euler-Lagrange approach [25, 41] as follows:

$$\partial_\mu \left(\frac{\partial \mathcal{L}}{\partial (\partial_\mu \phi)} \right) - \frac{\partial \mathcal{L}}{\partial \phi} = 0. \quad (2)$$

We can calculate the energy-momentum tensor ($\mathcal{T}^{\mu\nu}$) from the Lagrangian density, which can be employed to determine the energy density (\mathcal{E}) and pressure (\mathcal{P}). The third component of the energy-momentum tensor $\langle \mathcal{T}^{jj} \rangle$ gives the pressure, and the zeroth component $\langle \mathcal{T}^{00} \rangle$ computes the energy of the system.

$$\mathcal{T}^{\mu\nu} = \sum_{\phi_a} \frac{\partial \mathcal{L}}{\partial (\partial_\mu \phi_a)} \partial^\nu \phi_a - g^{\mu\nu} \mathcal{L}. \quad (3)$$

$$\mathcal{P} = \frac{1}{3} \sum_{j=1}^3 \langle \mathcal{T}^{jj} \rangle, \quad (4)$$

$$\mathcal{E} = \langle \mathcal{T}^{00} \rangle. \quad (5)$$

The equation of motion for nucleons, mesons, and photons can be derived from the Lagrangian density defined in Eq. (1). In mean-field approximation, the meson and photon fields are replaced by their respective mean-field values, σ , ω^0 , ρ^0 , and A^0 as

$$\begin{aligned}
& \left[\left(i\alpha \cdot \nabla - g_{\omega N} \omega^0 - \frac{1}{2} g_{\rho N} \tau_{3N} \rho^0 - e \frac{1 + \tau_{3N}}{2} A^0 \right) \right. \\
& \left. - \beta (M_N - g_{\sigma N} \sigma) \right] \Psi_N = \epsilon_N \Psi_N.
\end{aligned} \quad (6)$$

where $\alpha^i = \gamma^0 \gamma^i$ ($i = 1, 2, 3$) and $\beta = \gamma^0$. The Euler-Lagrange equations for the ground-state expectation values of the mesons fields are

$$(-\Delta + m_\sigma^2) \sigma = \sum_N g_{\sigma N} \rho_{sN} - \frac{\bar{\kappa}}{2} g_{\sigma N}^3 \sigma^2 - \frac{\bar{\lambda}}{6} g_{\sigma N}^4 \sigma^3 + a_1 g_{\sigma N} g_{\omega N}^2 (\omega^0)^2 + a_2 g_{\sigma N}^2 g_{\omega N}^2 \sigma (\omega^0)^2 + b_1 g_{\sigma N} g_{\rho N}^2 (\rho^0)^2 + b_2 g_{\sigma N}^2 g_{\rho N}^2 \sigma (\rho^0)^2, \quad (7)$$

$$(-\Delta + m_\omega^2) \omega^0 = \sum_N g_{\omega N} \rho_N - \frac{\zeta}{6} g_{\omega N}^4 (\omega^0)^3 - 2a_1 g_{\sigma N} g_{\omega N}^2 \sigma \omega^0 - a_2 g_{\sigma N}^2 g_{\omega N}^2 \sigma^2 \omega^0 - \Lambda_v g_{\omega N}^2 g_{\rho N}^2 (\omega^0)^2, \quad (8)$$

$$(-\Delta + m_\rho^2) \rho^0 = \sum_N g_{\rho N} \tau_{3N} \rho_N - 2b_1 g_{\sigma N} g_{\rho N}^2 \sigma \rho^0 - b_2 g_{\sigma N}^2 g_{\rho N}^2 \sigma^2 \rho^0 - \Lambda_v g_{\omega N}^2 g_{\rho N}^2 (\omega^0)^2 \rho^0 - \frac{\xi}{6} g_\rho^4 (\rho^0)^3, \quad (9)$$

$$-\Delta A^0 = e \rho_p. \quad (10)$$

The baryon vector density ρ_N , scalar density ρ_{sN} , and charge density ρ_p are, respectively,

$$\rho_N = \langle \bar{\Psi}_N \gamma^0 \Psi_N \rangle = \frac{\gamma k_N^3}{6\pi^2}, \quad (11)$$

$$\rho_{sN} = \langle \bar{\Psi}_N \Psi_N \rangle = \frac{\gamma}{(2\pi)^3} \int_0^{k_N} d^3k \frac{M_N^*}{\sqrt{k^2 + M_N^{*2}}}, \quad (12)$$

$$\rho_p = \left\langle \bar{\Psi}_N \gamma^0 \frac{1 + \tau_{3N}}{2} \Psi_N \right\rangle, \quad (13)$$

where γ is the spin-isospin degeneracy. The Dirac effective mass for the nucleon ($N = n, p$) can be expressed as

$$M_N^* = M_N - g_{\sigma N} \sigma, \quad (14)$$

The energy density of the uniform matter within the framework of the RMF model is given by

$$\mathcal{E} = \sum_{j=N,\ell} \frac{1}{\pi^2} \int_0^{k_j} k^2 \sqrt{k^2 + M_j^{*2}} dk + \sum_N g_{\omega N} \omega^0 \rho_N + \sum_N g_{\rho N} \tau_{3N} \rho_N \rho^0 + \frac{1}{2} m_\sigma^2 \sigma^2 + \frac{\bar{\kappa}}{6} g_{\sigma N}^3 \sigma^3 + \frac{\bar{\lambda}}{24} g_{\sigma N}^4 \sigma^4 - \frac{\zeta}{24} g_{\omega N}^4 (\omega^0)^4 - \frac{\xi}{24} g_{\rho N}^4 (\rho^0)^4 - \frac{1}{2} m_\omega^2 (\omega^0)^2 - \frac{1}{2} m_\rho^2 (\rho^0)^2 - a_1 g_{\sigma N} g_{\omega N}^2 \sigma (\omega^0)^2 - \frac{1}{2} a_2 g_{\sigma N}^2 g_{\omega N}^2 \sigma^2 (\omega^0)^2$$

$$- b_1 g_{\sigma N} g_{\rho N}^2 \sigma (\rho^0)^2 - \frac{1}{2} b_2 g_{\sigma N}^2 g_{\rho N}^2 \sigma^2 (\rho^0)^2 - \frac{1}{2} \Lambda_v g_{\omega N}^2 g_{\rho N}^2 (\omega^0)^2 (\rho^0)^2. \quad (15)$$

The pressure of the uniform matter is given by

$$\mathcal{P} = \sum_{j=N,\ell} \frac{1}{3\pi^2} \int_0^{k_j} \frac{k^4 dk}{\sqrt{k^2 + M_j^{*2}}} - \frac{1}{2} m_\sigma^2 \sigma^2 - \frac{\bar{\kappa}}{6} g_{\sigma N}^3 \sigma^3 - \frac{\bar{\lambda}}{24} g_{\sigma N}^4 \sigma^4 + \frac{\zeta}{24} g_{\omega N}^4 (\omega^0)^4 + \frac{\xi}{24} g_{\rho N}^4 (\rho^0)^4 + \frac{1}{2} m_\omega^2 (\omega^0)^2 + \frac{1}{2} m_\rho^2 (\rho^0)^2 + a_1 g_{\sigma N} g_{\omega N}^2 \sigma (\omega^0)^2 + \frac{1}{2} a_2 g_{\sigma N}^2 g_{\omega N}^2 \sigma^2 (\omega^0)^2 + b_1 g_{\sigma N} g_{\rho N}^2 \sigma (\rho^0)^2 + \frac{1}{2} b_2 g_{\sigma N}^2 g_{\rho N}^2 \sigma^2 (\rho^0)^2 + \frac{1}{2} \Lambda_v g_{\omega N}^2 g_{\rho N}^2 (\omega^0)^2 (\rho^0)^2. \quad (16)$$

Here, the sum is taken over nucleons and leptons.

The total binding energy of finite nuclei is given by the various individual contributions:

$$E_{\text{total}}(\Psi, \bar{\Psi}, \sigma, \omega^0, \rho^0, A^0) = E_{\text{part}} + E_{\sigma L} + E_{\sigma NL} + E_{\omega L} + E_{\omega NL} + E_\rho + E_\delta + E_{\sigma\omega} + E_{\sigma\rho} + E_{\omega\rho} + E_c + E_{\text{pair}} + E_{\text{CM}}, \quad (17)$$

where E_{part} signifies the sum of the single-particle energies of the nucleons. The terms $E_{\sigma L}$, $E_{\sigma NL}$, $E_{\omega L}$, $E_{\omega NL}$, E_ρ , and E_c represent the contributions attributed to the corresponding meson fields including linear and nonlinear parts and Coulomb fields, respectively. The terms $E_{\sigma\omega}$, $E_{\sigma\rho}$, and $E_{\omega\rho}$ represent the contributions from the mixed interaction terms involving σ , ω , and ρ mesons. Additionally, the effects of the pairing contribution E_{pair} and center of mass correction E_{CM} have been considered.

$$E_{\text{part}} = \sum_i n_i^2 \epsilon_i, \quad (18)$$

$$E_{\sigma L} = -\frac{g_\sigma}{2} \int d^3r \rho_{sN}(r) \sigma(r), \quad (19)$$

$$E_{\sigma NL} = \frac{1}{2} \int d^3r \left\{ \frac{\bar{\kappa}}{3} g_{\sigma N}^3 \sigma(r)^3 + \frac{\bar{\lambda}}{12} g_{\sigma N}^4 \sigma(r)^4 \right\}, \quad (20)$$

$$E_{\omega L} = -\frac{g_\omega}{2} \int d^3r \rho_N(r) \omega^0(r), \quad (21)$$

$$E_{\omega NL} = \frac{\zeta}{24} \int d^3r g_{\omega N}^4 (\omega^0(r))^4, \quad (22)$$

$$E_\rho = -\frac{g_\rho}{2} \int d^3r \rho_3(r) \rho^0(r), \quad (23)$$

$$E_{\sigma\omega} = -\frac{1}{2} \int d^3r \left\{ 2a_1 g_{\sigma N} g_{\omega N}^2 \sigma(r) \omega^0(r)^2 + a_2 g_{\sigma N}^2 g_{\omega N}^2 (\sigma(r))^2 \omega^0(r)^2 \right\}, \quad (24)$$

$$E_{\sigma\rho} = -\frac{1}{2} \int d^3r \left\{ 2b_1 g_{\sigma N} g_{\rho N}^2 \sigma(r) \rho^0(r)^2 + b_2 g_{\sigma N}^2 g_{\rho N}^2 (\sigma(r))^2 \rho^0(r)^2 \right\}, \quad (25)$$

$$E_{\omega\rho} = -\frac{\Lambda_v}{2} \int d^3r g_{\omega N}^2 g_{\rho N}^2 (\omega^0(r))^2 (\rho^0(r))^2, \quad (26)$$

$$E_c = -\frac{e^2}{8\pi} \int d^3r \rho_p(r) A^0(r), \quad (27)$$

$$E_{\text{pair}} = -\Delta \sum_i \sqrt{n_i(1-n_i)}, \quad (28)$$

$$E_{\text{CM}} = -\frac{3}{4} \hbar \omega^0 = \frac{3}{4} \times [45A^{-1/3} - 25A^{-2/3}]. \quad (29)$$

Here, the occupation numbers n_i are introduced to account for the effects of pairing, which is important for open-shell nuclei. In the absence of pairing interactions, they have a value of one (zero) for the levels below (above) the Fermi surface. When pairing is considered, the occupancy values (n_i) are determined within the framework of the constant gap approximation (BCS) by the following relation [42]:

$$n_i = \frac{1}{2} \left(1 - \frac{\epsilon_i - \lambda}{\sqrt{(\epsilon_i - \lambda)^2 + \Delta^2}} \right). \quad (30)$$

The pairing correlation has a significant role in open-shell nuclei [43]. The influence of the pairing correlation is considerably apparent with the increase in the mass number of nuclei. We have incorporated pairing for the open shell nuclei by employing the BCS formalism with constant pairing gaps (Δ) obtained from the particle separation energies of neighboring nuclei [43–45]. In the calculation of pairing energy, we use a pairing window, *i.e.*, the sum over i in Eq. (28) is only extended up to the level where $\epsilon_i - \lambda \leq 2 \hbar \omega^0$. The center-of-mass correction to the total binding energy E_{CM} is calculated within the harmonic oscillator approximation, which yields $E_{\text{CM}} = -3/4 \hbar \omega^0$, and we take $\hbar \omega^0 = 45A^{-1/3} - 25A^{-2/3}$ MeV [46, 47].

The charge radius is calculated by using the relation [42]

$$r_{\text{ch}} = \sqrt{r_p^2 + 0.64}. \quad (31)$$

The factor 0.64 included in Eq. (31) accounts for the finite size effect of the proton. The excess number of neutrons in a finite nucleus yield an important finite nuclear observable called the neutron skin thickness.

$$\Delta r_{np} = \langle r^2 \rangle_n^{\frac{1}{2}} - \langle r^2 \rangle_p^{\frac{1}{2}} = R_n - R_p, \quad (32)$$

where R_n and R_p are the rms radii for neutron and proton distributions, respectively.

We use the simulated annealing technique [48, 49] to optimize the model coupling parameters (\mathbf{p}) occurring in Eq. (1) by observing χ^2 minimization, which is represented as

$$\chi^2(\mathbf{p}) = \frac{1}{N_{\text{data}} - N_{\text{par}}} \sum_{i=1}^{N_{\text{data}}} \frac{(\mathcal{O}_i^{\text{th}} - \mathcal{O}_i^{\text{exp}})^2}{\Delta \mathcal{O}_i^2}, \quad (33)$$

where N_{data} and N_{par} indicate the numbers of experimental data points and parameters to be fitted, $\mathcal{O}_i^{\text{th}}$ and $\mathcal{O}_i^{\text{exp}}$ denote the theoretical and experimental values, respectively, of a nuclear observable, and $\Delta \mathcal{O}_i$ indicates the value of adopted errors on the nuclear observables [50–52]. The optimal model parameters \mathbf{p}_0 are those that minimize the χ^2 function. After searching the optimized model parameters, we use statistical/covariance analysis to estimate theoretical uncertainty in coupling parameters and nuclear observables. The statistical analysis provides insights into the sensitivity of parameters and physical quantities, as well as their interrelation [16, 50, 51, 53]. The behavior of the χ^2 function near its minimum is characterized by the curvature matrix $M_{\alpha\beta}$. Mathematically, this is expressed as

$$M_{\alpha\beta} = (J^T J) = \sum_{i=1}^{N_{\text{data}}} \frac{1}{\Delta \mathcal{O}_i^2} \left(\frac{\partial \mathcal{O}_i^{\text{th}}}{\partial p_\alpha} \right)_{p_0} \left(\frac{\partial \mathcal{O}_i^{\text{th}}}{\partial p_\beta} \right)_{p_0}, \quad (34)$$

where J is the Jacobian matrix defined as

$$J_{i\alpha} = \frac{1}{\Delta \mathcal{O}_i} \frac{\partial \mathcal{O}_i^{\text{th}}}{\partial p_\alpha}. \quad (35)$$

The covariance of two physical quantities A and B is expressed as

$$\text{cov}(A, B) = \overline{\Delta A \Delta B} = \sum_{\alpha\beta} \left(\frac{\partial A}{\partial p_\alpha} \right)_{p_0} C_{\alpha\beta} \left(\frac{\partial B}{\partial p_\beta} \right)_{p_0}. \quad (36)$$

Here, $C_{\alpha\beta} = \chi^2(p_0) M_{\alpha\beta}^{-1} = \chi^2(p_0) (J^T J)^{-1}$ is the covariance matrix. We can compute the standard deviation, $\sqrt{\Delta A^2}$, in A from Eq. (36) by placing $B = A$. Finally, the correlation coefficient between any two physical quantities

(parameter or observable), A and B , is given by [50, 51, 54–55]

$$r_{AB} = \frac{\overline{\Delta A \Delta B}}{\sqrt{\overline{\Delta A^2} \overline{\Delta B^2}}}. \quad (37)$$

III. RESULTS AND DISCUSSION

We propose an effective interaction HPU4 for the RMF relativistic EDF that provides neutron star features within astrophysical limitations, with finite nuclear and bulk nuclear matter at saturation density, in agreement with experimental data. The resulting parameter set, henceforth referred to as HPU4, is listed in Table 2. The model parameters are optimized using experimental values of the binding energy and charge rms radii r_{ch} for sixteen spherical closed/open-shell nuclei (deformation $\beta = 0$) such as $^{16,24}\text{O}$, $^{40,48,54}\text{Ca}$, $^{56,68,78}\text{Ni}$, ^{88}Sr , ^{90}Zr , $^{100,116,132,138}\text{Sn}$, ^{144}Sm , and ^{208}Pb [45, 56, 57] in the fitting technique.

In Table 1, we have listed the experimental data for binding energies, charge radii, neutron skin thickness of ^{48}Ca , and maximum mass of a neutron star of astrophysical interest along with adopted errors (ΔO_i) that have been used in the fitting protocol to optimize the coupling parameters. The recent precise parity-violating electron scattering experiments for ^{48}Ca (CREX) [5] and ^{208}Pb (PREX-II) [6] provide a deep understanding of Δr_{np} . The CREX result has given $\Delta r_{np} (^{48}\text{Ca}) = 0.121 \pm 0.026$ fm [5], whereas PREX-II measured $\Delta r_{np} (^{208}\text{Pb}) = 0.283 \pm 0.071$ fm [6]. The larger value of Δr_{np} for ^{208}Pb favors a stiffer value of L_0 around ρ_0 and suggests a stiff EoS. This leads to a higher value of $R_{1.4}$ and $\Lambda_{1.4}$ corresponding to a $1.4M_\odot$ neutron star [26], whereas CREX results are favored by a somewhat smaller value of L_0 and suggest a much softer EoS.

In Table 2, we depict the proposed relativistic interaction for the HPU4 model. The theoretical uncertainties are also displayed in parentheses. For comparison, we have shown the coupling parameters for other accurately calibrated RMF models, NL3 [12], FSUGold [14], and FSUGold2 [15], which are consistent with finite nuclear properties, but NL3 and FSUGold2 do not support astrophysical constraints on $\Lambda_{1.4}$ from the GW170817 event, whereas the FSUGold model underestimates the neutron star maximum mass constraints of $\approx 2 M_\odot$. Moreover, as mentioned in Refs. [8, 19, 26, 27, 28, 41], reproducing Δr_{np} as observed from CREX and PREX-II altogether within RMF approach is difficult. The CREX results favor a smaller value of L_0 , whereas a larger value is suggested by PREX-II.

In this paper, we propose HPU4 relativistic interaction to study the effect of the CREX results on atomic nuclei, infinite nuclear matter, and compact star structure.

Table 1. Data used in fitting protocol, *i.e.*, experimental nuclear data on the total binding energies (BE) [45], charge radii (r_{ch}) [58], and neutron skin (Δr_{np}) for the ^{48}Ca nucleus [5], and maximum mass of the neutron star (M_{max}) (in M_\odot) [35]. The adopted errors (ΔO_i) [50–52] used for model optimization in the fitting data. The BE is given in MeV, whereas r_{ch} and Δr_{np} are in fm.

Nucleus	Data used in fitting protocol		
	Observables	Expt. Value	ΔO_i
^{16}O	BE	−127.62	4.0
	r_{ch}	2.699	0.04
^{24}O	BE	−168.96	2.0
	BE	−342.04	4.0
^{40}Ca	r_{ch}	3.478	0.042
	BE	−415.96	1.0
^{48}Ca	r_{ch}	3.477	0.04
	Δr_{np}	0.121	0.026
	BE	−445.365	3.0
^{54}Ca	BE	−484.00	5.0
^{68}Ni	BE	−590.40	2.0
^{78}Ni	BE	−642.56	3.0
	BE	−768.41	3.0
^{88}Sr	r_{ch}	4.224	0.02
	BE	−783.81	2.0
^{90}Zr	r_{ch}	4.269	0.04
^{100}Sn	BE	−825.10	3.0
	BE	−988.66	3.0
^{116}Sn	r_{ch}	4.625	0.02
	BE	−1102.22	2.0
^{132}Sn	r_{ch}	4.709	0.04
^{138}Sn	BE	−1120.28	2.0
	BE	−1195.77	2.0
^{144}Sm	r_{ch}	4.952	0.04
	BE	−1636.33	1.0
^{208}Pb	r_{ch}	5.501	0.04
Neutron star mass	M_{max}	2.08	0.07

Therefore, we have incorporated CREX data $\Delta r_{np} = 0.121 \pm 0.026$ fm [5] in our fitting protocol during the model optimization to restrict the value of L_0 and to observe its implications on Δr_{np} of ^{208}Pb , $R_{1.4}$, and $\Lambda_{1.4}$ of the $1.4M_\odot$ neutron star. We use $M_{\text{max}} = 2.08 \pm 0.07 M_\odot$ of the neutron star [35] in fit data to constrain the EoS in high-density regimes. According to Refs. [17, 25, 36, 40], the fourth order self-interaction of the ω meson, measured using the coupling ζ , plays a key role in calculating the soft and stiff behavior of the EoS in high-density regimes.

Table 2. Model parameters for the newly optimized HPU4 model along with accurately calibrated RMF models: NL3 [12], FSUGold [14], and FSUGold2 [15]. Theoretical uncertainties are also given in parentheses. The parameters $g_{\sigma N}$, $g_{\omega N}$, $g_{\rho N}$, $\bar{\lambda}$, a_2 , b_2 , ζ , and Λ_v are dimensionless. The couplings $\bar{\kappa}$, a_1 , and b_1 are represented in units of fm^{-1} . The nucleon and meson masses M_N , m_σ , m_ω , and m_ρ are all given in MeV. The coupling parameters $\bar{\kappa}$, $\bar{\lambda}$, a_1 , a_2 , b_1 , and b_2 are expressed in $(\times 10^{-2})$.

Parameters	HPU4	NL3	FSUGold	FSUGold2
$g_{\sigma N}$	10.41443 (0.05179)	10.21743	10.59265	10.39532
$g_{\omega N}$	13.21616 (0.06147)	12.86762	14.30241	13.55413
$g_{\rho N}$	15.19767 (5.12104)	8.94800	11.76733	8.97026
$\bar{\kappa}$	2.22789 (0.09490)	1.95734	0.71961	1.52185
$\bar{\lambda}$	-0.03173 (0.21931)	-1.59136	2.37646	-0.05362
a_1	0.14718 (0.00757)	—	—	—
a_2	0.03293 (0.04967)	—	—	—
b_1	0.54871 (1.41277)	—	—	—
b_2	0.03254 (1.27634)	—	—	—
Λ_v	0.12590 (0.11553)	—	0.06000	0.00165
ζ	0.01968 (0.00412)	—	0.06000	0.02560
m_σ	507.445 (2.367)	508.194	491.500	497.479
m_ω	782.500	782.501	782.500	782.500
m_ρ	770.000	763.000	763.000	763.000
M_N	939.000	939.000	939.000	939.000

An increase in the coupling ζ [17, 25, 36, 40] causes a decrease in the neutron-star mass. Thus, by considering the M_{max} of the compact star in the fitting data during the model optimization, ζ , and hence, the softness and stiffness of the EoS at a high-density regime can be constrained. The value of χ^2 obtained after optimizing the HPU4 model parameters following Eq. (33) in minimization procedure, is determined as 1.04. For comparison, the χ^2 values obtained for other models considered in this

paper, such as NL3, FSUGold, FSUGold2, BigApple, DOPS3, and HPUC are 6.08, 6.25, 2.69, 13.43, 1.44, and 1.14, respectively, by following the similar process and using experimental data with adopted errors as given in Table 1.

In Table 3, we summarize the theoretical prediction for ground state properties such as B/A , r_{ch} , and Δr_{np} for some finite nuclei obtained using the newly proposed HPU4 interaction. For comparison, the results calculated for various parameter sets NL3 [12], FSUGold [14], FSUGold2 [15], DOPS3 [18], BigApple [16], and HPUC [59] are also displayed. The table shows that the theoretical predictions of B/A and r_{ch} agree well with their experimental counterparts. The rms errors in the total binding energy and charge radii for all nuclei in our fitting data are 2.43 MeV and 0.03 fm, respectively. For HPU4 parametrization, the values of Δr_{np} for $^{48}\text{Ca} = 0.146 \pm 0.019$ fm and satisfies the CREX results [5] within the error bar. HPU4 yields Δr_{np} for $^{208}\text{Pb} = 0.120 \pm 0.025$ fm and significantly underestimates the value of Δr_{np} for ^{208}Pb as reported recently by PREX-II [6]. The value obtained for $\Delta r_{np}(^{208}\text{Pb}) = 0.120 \pm 0.025$ fm for the HPU4 model is close as reported in Refs. [8, 19, 27, 52] and also agrees with the result reported for $\Delta r_{np} = 0.18 \pm 0.07$ fm for ^{208}Pb obtained using dispersive optical model analysis of the Washington University group [60]. This investigation suggests that by including $\Delta r_{np}(^{48}\text{Ca}) = 0.121 \pm 0.026$ from CREX data [5] in our fitting data to constrain the L_0 , a smaller value of $(\Delta r_{np}(^{208}\text{Pb}) = 0.120 \pm 0.025$ fm) for ^{208}Pb is obtained for the HPU4 model and underestimates the PREX-II results significantly [6]. This might be because the PREX-II results favor larger values of J_0 and L_0 , suggesting a stiffer EoS, whereas CREX results suggest a slightly smaller value of L_0 and a much softer EoS, as discussed in [8, 19, 27, 28, 52].

The theoretical results of Δr_{np} for ^{48}Ca and ^{208}Pb obtained for the HPU4 model satisfy the experimental results (^{48}Ca (RCNP) = 0.14 ± 0.20 fm [61], $^{208}\text{Pb} = 0.156^{+0.025}_{-0.021}$ fm [62], and ^{208}Pb (MAMI) = $0.15 \pm 0.03(\text{sat.})^{+0.01}_{-0.03}(\text{sys.})$ fm [63]). Δr_{np} values for ^{208}Pb calculated using the HPU4 model are also consistent with the value $\Delta r_{np} = (0.18 \pm 0.07)$ fm for ^{208}Pb obtained by the Washington University group as reflected in [60]. Δr_{np} predicted using the HPU4 model underestimates the PREX-II results, and tension for simultaneously reproducing PREX-II and CREX results continues, as discussed in Ref. [8, 19, 27, 28]. According to Refs. [8, 19], reproducing the CREX and PREX-II results for Δr_{np} altogether using RMF models is challenging. The CREX results suggest a smaller value of L_0 whereas PREX-II results favor a stiffer value as illustrated in detail in the above references. Other models considered in the present calculation also do not simultaneously satisfy these results for Δr_{np} for ^{208}Pb and ^{48}Ca . Recent studies on non-relativistic and RMF models have observed similar characteristics, highlighting the

Table 3. Theoretical results for ground state properties (binding energy per nucleon B/A (in MeV), charge radii r_{ch} (in fm) and neutron skin Δr_{np} (in fm) obtained with HPU4, NL3, FSUGold, FSUGold2, and HPUC models. Available experimental values of B/A [45] and r_{ch} [58], and Δr_{np} [5, 6, 60, 65] for the nuclei are also shown for comparison.

Nucleus	Observable	Experiment	HPU4	NL3	FSUGold	FSUGold2	HPUC
¹⁶ O	B/A	7.98	8.16	7.94	7.87	7.89	8.13
	r_{ch}	2.699	2.676	2.728	2.686	2.707	2.696
	Δr_{np}	—	−0.029	−0.028	−0.028	−0.028	−0.029
²⁴ O	B/A	7.04	7.01	7.10	6.88	7.09	6.96
	r_{ch}	—	2.748	2.737	2.732	2.718	2.762
	Δr_{np}	—	0.535	0.636	0.627	0.649	0.540
⁴⁰ Ca	B/A	8.55	8.62	8.53	8.52	8.52	8.62
	r_{ch}	3.478	3.424	3.470	3.434	3.448	3.445
	Δr_{np}	0.08 ^{+0.05} _{−1.0}	−0.052	−0.048	−0.051	−0.049	−0.051
⁴⁸ Ca	B/A	8.67	8.67	8.63	8.57	8.62	8.66
	r_{ch}	3.477	3.462	3.471	3.460	3.449	3.478
	Δr_{np}	0.121± 0.026	0.146	0.226	0.197	0.232	0.147
⁵⁴ Ca	B/A	8.25	8.19	8.21	8.12	8.22	8.16
	r_{ch}	—	3.553	3.537	3.533	3.512	3.570
	Δr_{np}	—	0.442	0.571	0.539	0.587	0.455
⁵⁶ Ni	B/A	8.64	8.58	8.60	8.52	8.58	8.60
	r_{ch}	—	3.698	3.716	3.724	3.702	3.708
	Δr_{np}	0.03 ^{+0.08} _{−0.11}	−0.038	−0.034	−0.038	−0.035	−0.037
⁶⁸ Ni	B/A	8.68	8.71	8.69	8.67	8.69	8.72
	r_{ch}	—	3.871	3.862	3.864	3.841	3.889
	Δr_{np}	—	0.223	0.333	0.287	0.339	0.227
⁷⁸ Ni	B/A	8.24	8.24	8.24	8.15	8.22	8.22
	r_{ch}	—	3.965	3.942	3.957	3.925	3.980
	Δr_{np}	—	0.382	0.554	0.495	0.566	0.390
⁸⁸ Sr	B/A	8.73	8.72	8.71	8.70	8.71	8.72
	r_{ch}	4.224	4.225	4.225	4.220	4.203	4.238
	Δr_{np}	—	0.063	0.148	0.113	0.152	0.068
⁹⁰ Zr	B/A	8.71	8.69	8.69	8.68	8.69	8.70
	r_{ch}	4.269	4.270	4.280	4.274	4.258	4.289
	Δr_{np}	0.090± 0.020	0.033	0.097	0.069	0.099	0.033
¹⁰⁰ Sn	B/A	8.25	8.22	8.29	8.24	8.28	8.24
	r_{ch}	—	4.502	4.511	4.519	4.495	4.516
	Δr_{np}	—	−0.136	−0.117	−0.127	−0.120	−0.133
¹¹⁶ Sn	B/A	8.52	8.50	8.50	8.51	8.51	8.51
	r_{ch}	4.625	4.612	4.610	4.611	4.588	4.634
	Δr_{np}	0.100± 0.030	0.087	0.183	0.142	0.188	0.088
¹³² Sn	B/A	8.36	8.36	8.37	8.34	8.36	8.36
	r_{ch}	4.710	4.729	4.711	4.725	4.692	4.749
	Δr_{np}	—	0.215	0.383	0.310	0.391	0.217

Continued on next page

Table 3-continued from previous page

Nucleus	Observable	Experiment	HPU4	NL3	FSUGold	FSUGold2	HPUC
^{138}Sn	B/A	8.12	8.11	8.37	8.08	8.12	8.09
	r_{ch}	—	4.792	4.756	4.773	4.735	4.809
	Δr_{np}	—	0.330	0.544	0.461	0.556	0.346
^{144}Sm	B/A	8.30	8.29	8.32	8.33	8.32	8.31
	r_{ch}	4.952	4.957	4.956	4.957	4.934	4.980
	Δr_{np}	—	0.043	0.138	0.096	0.142	0.044
^{208}Pb	B/A	7.87	7.86	7.88	7.89	7.89	7.88
	r_{ch}	5.501	5.532	5.517	5.529	5.489	5.556
	Δr_{np}	0.283 ± 0.071 [6] 0.18 ± 0.07 [60]	0.120	0.279	0.207	0.286	0.119

need for more experimental investigations. [8, 28, 64].

Table 4 depicts nuclear matter parameters such as the binding energy per nucleon (E/A), incompressibility coefficient (K), effective mass ratio (M^*/M) at saturation density (ρ_0), symmetry energy (J_0), slope of symmetry energy (L_0), and curvature of J , *i.e.*, K_{sym} along with the theoretical errors. We also display the Δr_{np} values for ^{48}Ca and ^{208}Pb . Nuclear matter characteristics significantly influence the asymmetric nuclear dense matter EoS. For the proposed HPU4 model, we find that the isoscalar nuclear matter parameters are constrained well (at the uncertainty $\leq 3.4\%$). The error on L_0 is relatively larger ($\approx 33\%$). As reported in [66–68], K_{sym} is poorly determined, and the available finite nuclear experimental data are not sufficient to restrict the value of K_{sym} . We can constrain K_{sym} in tighter limits only if we have precise knowledge of J at higher densities, *i.e.*, $\rho > 2\rho_0$. We observe that the value of K_{sym} for the HPU4 model overlaps with the theoretical analysis within the error bar, $K_{\text{sym}} = -107 \pm 88$

MeV [69]. The HPU4 model has an E/A value of -15.94 MeV. J_0 and L_0 calculated for HPU4 model agree well with $J_0 = 29.1^{+2.1(3.6)}_{-1.8(2.7)}$ MeV and $L_0 = 17.1^{+23.8(39.3)}_{-22.3(36.0)}$ MeV inferred by Zhang *et al.* [27] and $L_0 = 50 \pm 12$ MeV [70]. The value of $K = 228.67 \pm 7.88$ MeV for the HPU4 parameter set satisfies $K = 240 \pm 20$ MeV as reported in [71, 72].

Figure 1 depicts the coefficients of correlation (in graphical form) for the HPU4 model parametrization occurring in Equation (1). The isoscalar coupling $g_{\sigma N}$ is found to exhibit a moderate to strong correlation with the model parameters $g_{\omega N}$, $\bar{\kappa}$, a_1 , a_2 , and m_σ . The isoscalar coupling parameter $g_{\omega N}$ also exhibits dependence on a_1 and a_2 . A good correlation also exists between pair of model parameters $a_1 - \bar{\kappa}$ and $a_1 - m_\sigma$. We also notice a strong correlation for isovector coupling $g_{\rho N}$ with Λ_v and b_1 . The parameter Λ_v also exhibits strong dependence on b_1 as observed from their coefficient of correlation. If two model parameters exhibit a strong coefficient of correlation,

Table 4. Bulk nuclear matter properties at saturation density along with theoretical uncertainties (within the parenthesis) obtained for the HPU4 model. Here, ρ_0 , E/A , K , M^*/M , J_0 , L_0 , and K_{sym} denote the saturation density, binding energy per nucleon, nuclear matter incompressibility, ratio of effective nucleon mass to the nucleon mass, symmetry energy, linear density dependence of symmetry energy, and curvature of symmetry energy, respectively. Δr_{np} values for ^{48}Ca and ^{208}Pb are also shown. The results obtained with various accurately calibrated RMF Models are also shown for comparison.

Properties	HPU4	NL3	FSUGold	FSUGold2	DOPS3	BigApple	HPUC
ρ_0/fm^{-3}	0.1506 (0.004)	0.1481	0.1484	0.1504	0.1480	0.1550	0.1490
$E/A/\text{MeV}$	-15.94 (0.04)	-16.23	-16.23	-16.28	-16.04	-16.34	-15.98
K/MeV	228.67 (7.88)	271.45	230.04	237.86	227.65	227.09	220.19
M^*/M	0.619 (0.008)	0.595	0.610	0.593	0.605	0.608	0.610
J_0/MeV	27.92 (1.31)	37.26	32.59	37.58	31.77	31.41	28.37
L_0/MeV	42.86 (14.26)	118.15	60.55	112.70	66.69	40.33	41.64
$K_{\text{sym}}/\text{MeV}$	55.13 (73.12)	100.96	-51.30	25.39	-0.62	89.59	81.12
$\Delta r_{\text{np}}(^{48}\text{Ca})/\text{fm}$	0.146 (0.019)	0.226	0.197	0.232	0.184	0.168	0.147
$\Delta r_{\text{np}}(^{208}\text{Pb})/\text{fm}$	0.120 (0.025)	0.279	0.207	0.286	0.188	0.151	0.119

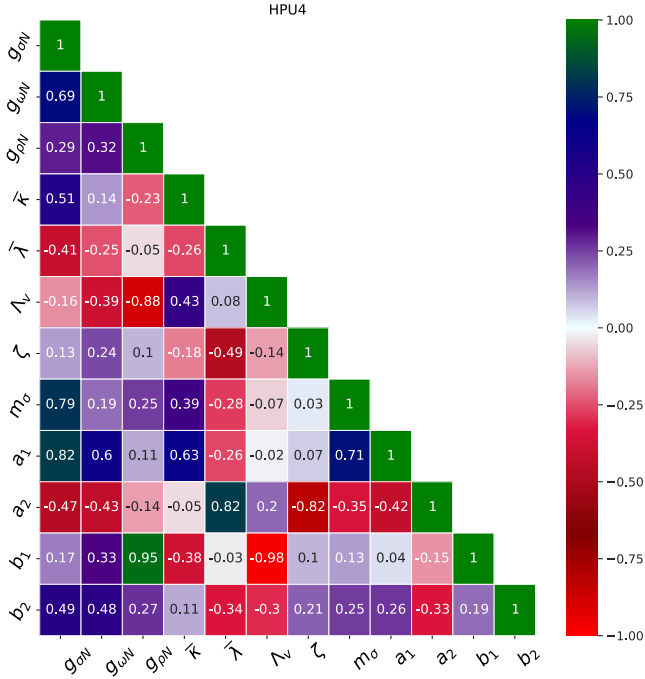


Fig. 1. (color online) Graphical representation of coefficients of correlation between coupling terms for HPU4 model.

tion, this implies that the parameters are strongly interdependent. The parameter ζ also shows strong dependence on a_2 . The very strong correlation observed between isoscalar couplings $g_{\sigma N}$ and $g_{\omega N}$, as reported in [41, 54], becomes somewhat smaller for the HPU4 model. This might be because, in this model, these couplings also exhibit good correlations with the mixed interaction terms a_1 ($\sigma - \omega^2$) and a_2 ($\sigma^2 - \omega^2$) included in the Lagrangian of HPU4 model. The strong dependence of isovector coupling g_ρ on cross interaction parameters b_1 ($\sigma - \rho^2$) and Λ_v ($\omega^2 - \rho^2$) is also observed.

Figure 2 depicts a plot of J versus (ρ/ρ_0) for the HPU4 parametrization. For comparison, the results for various parameter sets NL3 [12], FSUGold [14], FSUGold2 [15], DOPS3 [18], BigApple [16], and HPUC [59] are considered. The various constraints imposed on J as reported in Refs. [73, 74] are also displayed by shaded regions. We observe that the value of J increases with ρ for the parameter sets considered and satisfies the constraints mentioned in [73, 74]. J at $2\rho_0$ for the HPU model is found to be $J(2\rho_0) = 45.06$ MeV. It is consistent with $J(2\rho_0) = 51 \pm 13$ MeV [69] and $J(2\rho_0) = 40.2 \pm 12.8$ MeV, as reported in [53]. For the HPU4 model, we obtain the softest J around ρ_0 . This is because we obtain a larger value of the coupling parameter Λ_v during the HPU4 model optimization, and Λ_v is observed to have a significant contribution to constrain J and L .

To calculate the mass and radius of a non-rotating compact star, we solve the Tolman-Oppenheimer-Volkoff (TOV) equations, which are Einstein's equations for stat-

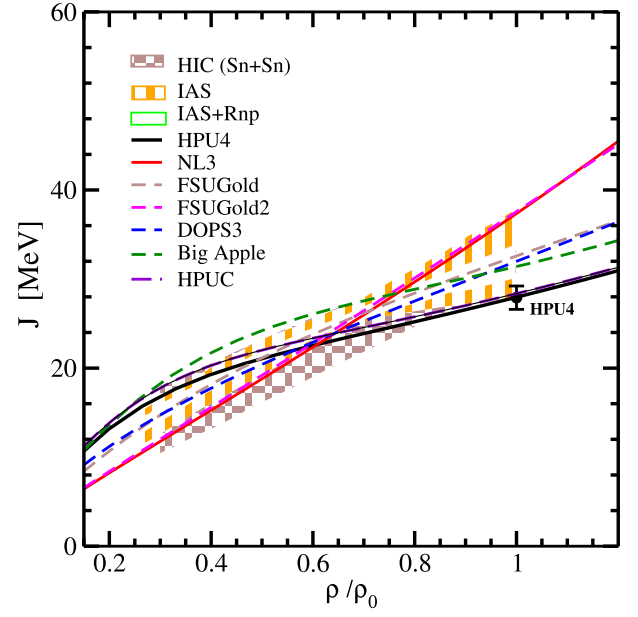


Fig. 2. (color online) Dependence of J on ρ/ρ_0 for the HPU4 model and other RMF models. The theoretical uncertainty for J at saturation density calculated for the HPU4 model is also shown.

ic and spherically symmetric stars [75, 76]:

$$\frac{d\mathcal{P}(r)}{dr} = -\frac{[\mathcal{E}(r) + \mathcal{P}(r)][4\pi r^3 \mathcal{P}(r) + m(r)]}{r^2(1 - 2m(r)/r)}. \quad (38)$$

The mass of a compact star $m(r)$ enclosed in a sphere of radius r is related to its energy density using the relation

$$\frac{dm}{dr} = 4\pi r^2 \mathcal{E}(r), \quad (39)$$

for a given EoS $\mathcal{P}(\epsilon)$, differential Eqs. (38) and (39) can be solved simultaneously. The total mass of a compact star is

$$m(r) = 4\pi \int_0^r dr r^2 \mathcal{E}(r). \quad (40)$$

When estimating neutron star parameters, we must consider the EoS of the crust, which governs the low-density regime. The radius of a $1.4M_\odot$ neutron star is particularly sensitive to the crust EoS. In this work, we employ the Baym-Pethick-Sutherland (BPS) EoS [77] for the crust region.

Figure 3 shows the mass-radius relationship for static stars using the HPU4 model. We also show the computed results for various models. M_{\max} of a non-rotating neutron star in the HPU4 model is found to be $2.03 \pm 0.04 M_\odot$, which satisfies the mass constraints reported in [3, 4, 31, 34, 78]. $R_{1.4}$ of canonical mass neutron star including

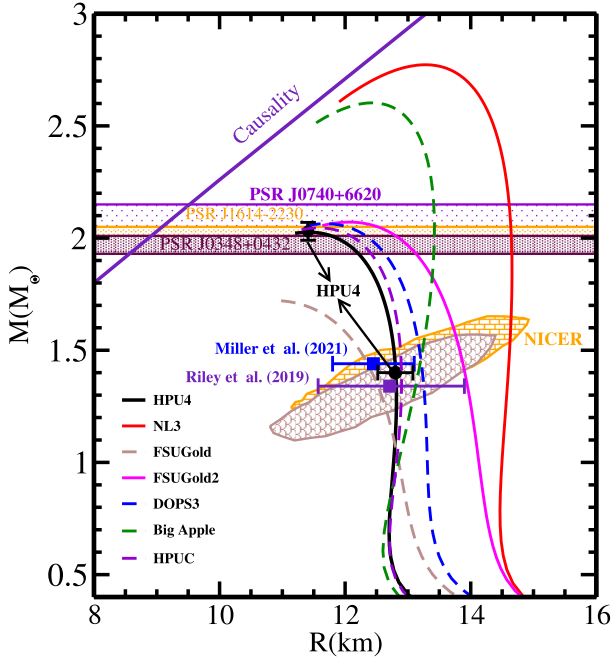


Fig. 3. (color online) Neutron star mass-radius relationship for various parametrizations considered in this paper. Mass constraints of PSR J1614-2230, PSR J0348+0432, and PSR J0740+6620 [31, 34, 35] are indicated by horizontal bands. Constraints from NICER measurements [3, 29] and theoretical uncertainties on M_{\max} and $R_{1.4}$ calculated for the HPU4 model are also shown.

a BPS crust [77] is 12.80 ± 0.28 Km, which is consistent with the constraints from NICER on $R_{1.4}$. The computed mass-radius of a neutron star with HPU4 parameterization aligns with NICER measurements [3, 4] as shown in the shaded regions in Fig. 3. $R_{1.4}$ also corresponds with radius limits from NICER measurements [3, 4, 79].

Figure 4 shows the variation in the dimensionless tidal deformability $\Lambda_{1.4}$ [81–83] with $R_{1.4}$ for HPU4 and other models. Note that the value of $\Lambda_{1.4}$ calculated for the HPU4 interaction is 556.60 ± 33.67 , which satisfies $\Lambda_{1.4} \leq 580$ for the GW170817 event with a 90% confidence level [1] and is also consistent with the findings reported in Ref. [69]. This might be owing to the inclusion of CREX results in our fitting protocol during the model optimization that results in soft symmetry energy with its value of linear density dependence $L_0 = 42.85 \pm 14.26$ MeV. $\Lambda_{1.4}$ strongly interrelates with $R_{1.4}$. The observed $\Lambda_{1.4}$ from GW170817 favors the small value of $R_{1.4}$ and, hence, a smaller value of L_0 .

Table 5 summarizes HPU4 model results for several characteristics of non-rotating neutron stars. The theoretical uncertainties on the neutron star observables calculated using Eqs. (36) and (37) are also listed. We have also shown the results with other models. Table 5 shows that very small theoretical uncertainties on M_{\max} (1.97 %), R_{\max} (0.96 %), and $R_{1.4}$ (2.18 %) of neutron star are

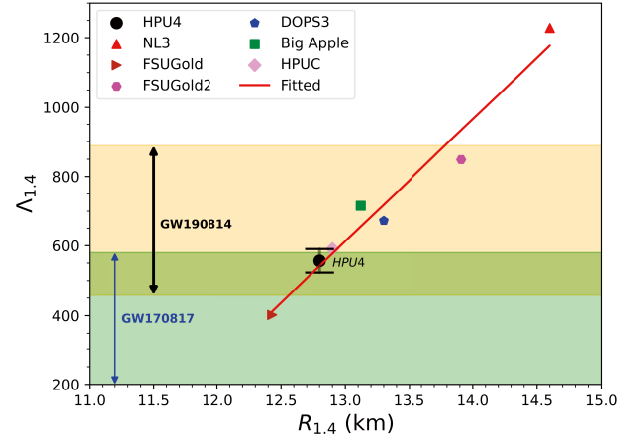


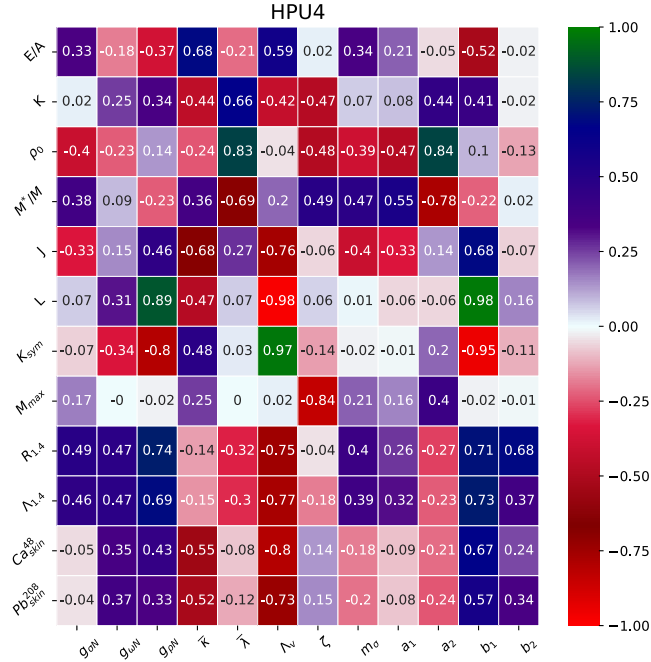
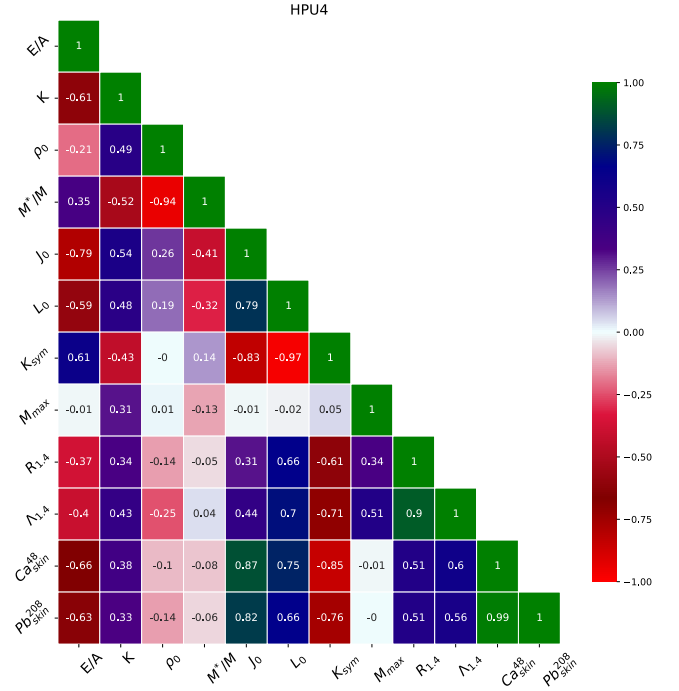
Fig. 4. (color online) Correlation between $\Lambda_{1.4}$ and $R_{1.4}$. The solid line indicates the fitting line given by $\Lambda_{1.4} = 2.088 \times 10^{-4} (R_{1.4}/\text{km})^{5.81}$. The constraints on $\Lambda_{1.4}$ from GW170817 ($\Lambda_{1.4} = 190^{+390}_{-120}$) [1] and GW190814 ($\Lambda_{1.4} = 616^{+273}_{-158}$) [80] and theoretical uncertainty on $\Lambda_{1.4}$ calculated with the HPU4 model are also shown.

obtained for the HPU4 model. The small uncertainties may be because M_{\max} has been included in the fitting data during the optimization to constrain the EoS in the high-density regime, which constrains the coupling ζ . The increased error (≈ 6 %) for $\Lambda_{1.4}$ may be because $\Lambda \propto R^5$, showing that an accurate Λ measurement can constrain the radius of a compact star within narrower boundaries. To date, researchers assume that no terrestrial experiments can accurately constrain dense matter mass-radius [26].

Figure 5 shows a graphical representation of the correlation between observables of nuclear matter and neutron stars with HPU4 model parameters. We can observe from Fig. 5 that observables such as M^*/M , E/A , and K exhibit moderate to strong correlations with coupling terms $\bar{\lambda}$, $\bar{\kappa}$, Λ_v , a_1 , a_2 , and b_1 . Weak correlations between M^*/M , E/A , and K , and isoscalar parameters $g_{\sigma N}$, $g_{\omega N}$, and $g_{\rho N}$ is observed when mixed interaction terms a_1 , a_2 , b_1 , b_2 , and Λ_v are included in the Lagrangian of HPU4 model. Additionally, the values of J_0 , L_0 , and K_{sym} can be constrained well by the couplings Λ_v , b_1 , and $g_{\rho N}$ as indicated by their correlations. The parameters Λ_v and b_1 can be used to constrain the Δr_{np} for ^{208}Pb and ^{48}Ca nuclei as they have strong correlations between each other. The HPU4 model exhibits a significant negative correlation of M_{\max} with ω -meson self-coupling ζ , as expected. $R_{1.4}$ and $\Lambda_{1.4}$ are strongly correlated with g_{ρ} and mixed coupling terms Λ_v , b_1 , and b_2 incorporated in the HPU4 model. We observe that the correlations of nuclear matter properties in the isovector sector such as J_0 , L_0 , K_{sym} , neutron star observables $R_{1.4}$, $\Lambda_{1.4}$ and neutron skin of ^{48}Ca and ^{208}Pb with couplings $g_{\rho N}$ and Λ_v weaken in the HPU4 model compared with the HPUC model [59]. This might be because, for the HPU4 model, the mixed inter-

Table 5. Properties of nonrotating neutron stars calculated for the HPU4 parameter set. Theoretical uncertainties are also shown within the parenthesis. The results obtained with other RMF models are also shown for comparison.

Properties	HPU4	NL3	FSUGold	FSUGold2	DOPS3	BigApple	HPUC
M_{\max} (M_{\odot})	2.03 (0.04)	2.77	1.72	2.07	2.07	2.60	2.04
R_{\max} /km	11.41 (0.11)	12.74	10.98	11.87	11.61	12.15	11.57
$R_{1.4}$ /km	12.80 (0.28)	14.60	12.45	13.91	13.30	13.12	12.90
$\Lambda_{1.4}$	556.60 (33.67)	1228.38	401.99	848.97	672.07	715.96	590.83

**Fig. 5.** (color online) Graphical view of coefficients of correlation between the nuclear observables and parameters of the HPU4 model.**Fig. 6.** (color online) Graphical view of coefficients of correlation amongst nuclear observables for the HPU4 model.

action of σ - ρ mesons in addition to $g_{\rho N}$ and Λ_v are incorporated, which also constrain J , L , and Δr_{np} and the behavior of the EoS in the high-density regime. The dependence of these nuclear matter and neutron star observables on mixed interactions of σ - ρ mesons is also evident from their coefficients of correlation with b_1 (σ - ρ^2) and b_2 (σ^2 - ρ^2).

In Fig. 6, we depict a graphical view of the coefficients of correlation amongst nuclear matter parameters, neutron star observables, and neutron skin thickness, Δr_{np} , of ^{208}Pb and ^{48}Ca nuclei. The Δr_{np} values of ^{208}Pb and ^{48}Ca exhibit a strong correlation and show a strong dependence on J_0 , L_0 , and K_{sym} , as can be observed from their correlations. $R_{1.4}$ and $\Lambda_{1.4}$ are strongly intercorrelated (see Fig. 4). The radius $R_{1.4}$ shows a strong dependence on L_0 and K_{sym} . These results are in close agreement with those in Refs. [53, 54]. K_{sym} is also strongly correlated with $R_{1.4}$ and $\Lambda_{1.4}$.

Note that in this work, PREX-II results have not been considered in the fitting protocol for model optimization.

$\Delta r_{np} = 0.283 \pm 0.071$ fm for ^{208}Pb reported from PREX-II favors a stiffer value of L around ρ_0 and suggests a stiff EoS that generally leads to a larger value of $R_{1.4}$ and $\Lambda_{1.4}$ and does not satisfy the revised limit $\Lambda_{1.4} \leq 580$ for the GW170817 event [1]. The contribution from the nucleon- δ meson interaction in the Lagrangian affects the properties of asymmetric nuclear dense matter and plays an important role in understanding the astrophysical observations of neutron stars. The nucleon- δ meson coupling stiffens the nuclear EoS above the saturation density [19, 52]. In this study, we have focused on cross-couplings of σ , ω , and ρ mesons to constrain J_0 and L_0 values and soften EoSs, rather than the nucleon- δ meson interaction (coupling term g_δ) in the Lagrangian. We observe that, in the absence of contribution from the δ meson in the Lagrangian, a comparatively larger value of mixed interaction term of ω^2 - ρ^2 quantified by the coupling Λ_v is required to constrain the values of J_0 and L_0 when the CREX results are incorporated in the fitting protocol for the model optimizations.

Additionally, $R_{1.4}$ shows good dependence on mixed interaction terms b_1 (σ - ρ^2) and b_2 (σ^2 - ρ^2). Here, we have coupling terms $g_{\rho N}$, b_1 , b_2 , and Λ_v to constrain J_0 and L_0 . The cross-coupling terms of mesons are important to reconcile model parameter's naturalness behavior with the EFT [24]. Furthermore, the inclusion of the cross-interaction couplings in the Lagrangian has significant effects on the values of L and provides comparatively softer EoSs in the medium density regime (required for canonical neutron star mass) and satisfies the revised limit $\Lambda_{1.4} \leq 580$ inferred from the GW170817 event as reported in [1].

IV. SUMMARY

We have constructed a HPU4 interaction using the RMF model with various nucleon-meson couplings by taking the binding energies, charge rms radii of finite nuclei, and neutron skin of ^{48}Ca from CREX collaborations for the observed mass of astrophysical objects of interest in the fitting technique. The effective interaction illustrates the implications of the CREX results on finite, symmetric, and asymmetric dense matter. The ground state properties calculated with the HPU4 model, such as binding energies and charge radii, correspond well with experimental results. The rms error of total binding energies and charge radii (r_{ch}) for finite nuclei used in the fitting process are 2.43 MeV and 0.03 fm, respectively.

We have also performed a covariance analysis, which aids in estimating the statistical errors on the coupling parameters and physical observables, as well as correla-

tions among them. The Δr_{np} values for ^{208}Pb and ^{48}Ca are strongly correlated and show a strong dependence on isovector nuclear parameters J_0 , L_0 , and K_{sym} , as can be observed from their correlation coefficients. We obtain $\Delta r_{np} = 0.146 \pm 0.019$ fm for ^{48}Ca with a soft symmetry energy ($J_0 = 27.91 \pm 1.31$ MeV) and its corresponding linear density dependence ($L_0 = 42.85 \pm 14.26$ MeV) at saturation density, which is consistent with the CREX results. We obtain $\Delta r_{np} = 0.120 \pm 0.025$ fm for ^{208}Pb , which is significantly underestimated from the PREX-II values and agrees with the findings reported in [8, 19, 27, 52]. For the HPU4 model, the value of neutron star's M_{max} and $R_{1.4}$ are $2.03(0.04) M_{\odot}$ and $12.80(0.28)$ km, respectively. The value of $\Lambda_{1.4}$ equal to 556.60 ± 33.67 obtained for HPU4 parameterization overlaps with the revised constraint ($\Lambda_{1.4} \leq 580$) from the GW170817 event [1]. The results of this study show that, although the mixed interaction terms of σ , ω , and ρ mesons influence the asymmetric nuclear dense matter, they have less impact on finite nuclear properties when the appropriate calibration of coupling parameters is obtained. A strong correlation of $R_{1.4}$ with ρ - N coupling g_{ρ} , and mixed interaction terms, $\sigma\rho_{\mu}\rho^{\mu}$ and $\sigma^2\rho_{\mu}\rho^{\mu}$ is also observed.

ACKNOWLEDGEMENTS

Author(s) are highly thankful to Himachal Pradesh University (HPU) for giving access to the computational facilities.

References

- [1] B. P. Abbott, R. Abbott, T. D. Abbott *et al.*, *Phys. Rev. Lett.* **121**(16), 161101 (2018)
- [2] B. P. Abbott *et al.* (LIGO Scientific Collaboration and Virgo Collaboration), *Phys. Rev. X* **9**, 011001 (2019)
- [3] M. Miller, F. Lamb, A. Dittmann *et al.*, *Astrophys. J. Lett.* **918**, L28 (2021)
- [4] T. E. Riley, A. L. Watts, P. S. Ray *et al.*, *Astrophys. J. Lett.* **918**, L27 (2021)
- [5] Adhikari D e a (CREX Collaboration), *Phys. Rev. Lett.* **129**(4), 042501 (2022)
- [6] D. Adhikari, H. Albatineh, D. Androic *et al.*, *Phys. Rev. Lett.* **126**, 172502 (2021)
- [7] P. G. Reinhard, X. Roca-Maza, and W. Nazarewicz, *Phys. Rev. Lett.* **127**(23), 232501 (2021)
- [8] P. G. Reinhard, X. Roca-Maza, and W. Nazarewicz, *Phys. Rev. Lett.* **129**(23), 232501 (2022)
- [9] T. Miyatsu, M. K. Cheoun, and K. Saito, *Phys. Rev. C* **88**, 015802 (2013)
- [10] S. Abrahamyan, Z. Ahmed, H. Albatineh *et al.*, *Phys. Rev. Lett.* **108**, 112502 (2012)
- [11] N. Glendenning and S. Moszkowski, *Phys. Rev. Lett.* **67**, 2414 (1991)
- [12] G. Lalazissis, J. König, and P. Ring, *Phys. Rev. C* **55**, 540 (1997)
- [13] Y. Sugahara and H. Toki, *Nucl. Phys. A* **579**, 557 (1994)
- [14] B. G. Todd-Rutel and J. Piekarewicz, *Phys. Rev. Lett.* **95**(12), 122501 (2005)
- [15] W. C. Chen and J. Piekarewicz, *Phys. Rev. C* **90**(4), 044305 (2014)
- [16] F. J. Fattoyev, C. J. Horowitz, J. Piekarewicz *et al.*, *Phys. Rev. C* **102**(6), 065805 (2020)
- [17] R. Kumar, M. Kumar, V. Thakur *et al.*, *Phys. Rev. C* **107**(5), 055805 (2023)
- [18] V. Thakur, R. Kumar, P. Kumar *et al.*, *Phys. Rev. C* **106**, 025803 (2022)
- [19] T. Miyatsu, M. K. Cheoun, K. Kim *et al.*, *Phys. Lett. B* **843**, 138013 (2023)
- [20] B. T. Reed, F. J. Fattoyev, C. J. Horowitz *et al.*, *Phys. Rev. C* **109**(3), 035803 (2024)
- [21] M. Kumar, S. Kumar, K. R. Queena *et al.*, *Phys. Rev. C* **110**(5), 055802 (2024)
- [22] N. Alam, A. Sulaksono, and B. K. Agrawal, *Phys. Rev. C* **92**(1), 015804 (2015)
- [23] R. Furnstahl, B. D. Serot, and H. B. Tang, *Nucl. Phys. A* **615**, 441 (1997)
- [24] R. Furnstahl, B. D. Serot, and H. B. Tang, *Nucl. Phys. A* **598**, 539 (1996)
- [25] S. K. Dhiman, R. Kumar, and B. K. Agrawal, *Phys. Rev. C* **76**, 045801 (2007)
- [26] B. T. Reed, F. J. Fattoyev, C. J. Horowitz *et al.*, *Phys. Rev.*

- Lett. **126**, 172503 (2021)
- [27] Z. Zhang and L. W. Chen, *Phys. Rev. C* **108**(2), 024317 (2023)
- [28] E. Yuksel and N. Paar, *Phys. Lett. B* **836**, 137622 (2023)
- [29] T. E. Riley, A. L. Watts, S. Bogdanov *et al.*, *Astrophys. J.* **887**, L21 (2019)
- [30] M. C. Miller, F. K. Lamb, A. J. Dittmann *et al.*, *Astrophys. J.* **887**, L24 (2019)
- [31] P. B. Demorest, T. Pennucci, S. M. Ransom *et al.*, *Nature* **467**, 1081 (2010)
- [32] J. Antoniadis, P. C. C. Freire, N. Wex *et al.*, *Science* **340**, 1233232 (2013)
- [33] Z. Arzoumanian, A. Brazier, S. Burke-Spolaor *et al.*, *Astrophys. J. Suppl. S.* **235**, 37 (2018)
- [34] L. Rezzolla, E. R. Most, and L. R. Weih, *Astrophys. J. Lett.* **852**, L25 (2018)
- [35] E. Fonseca, H. Cromartie, T. T. Pennucci *et al.*, *Astrophys. J. Lett.* **915**, L12 (2021)
- [36] H. Mueller and B. D. Serot, *Nucl. Phys. A* **606**, 508 (1996)
- [37] B. D. Serot and J. D. Walecka, *Adv. Nucl. Phys.* **16**, 1 (1986)
- [38] J. Boguta and A. Bodmer, *Nucl. Phys. A* **292**, 413 (1977)
- [39] J. Walecka, *Ann. Phys.* **83**, 491 (1974)
- [40] B. K. Pradhan, D. Chatterjee, R. Gandhi *et al.*, *Nucl. Phys. A* **1030**, 122578 (2023)
- [41] V. Thakur, R. Kumar, P. Kumar *et al.*, *Phys. Rev. C* **107**(1), 015803 (2023)
- [42] P. Ring, Y. Gambhir, and G. Lalazissis, *Com. Phys. Commun.* **105**, 77 (1997)
- [43] P. Ring and P. Schuck, *The nuclear many-body problem* (Springer Science & Business Media, 1980)
- [44] S. Karatzikos, A. Afanasjev, G. Lalazissis *et al.*, *Phys. Lett. B* **689**, 72 (2010)
- [45] M. Wang, W. Huang, F. G. Kondev *et al.*, *Chin. Phys. C* **45**, 030003 (2021)
- [46] R. Kumar, B. K. Agrawal, and S. K. Dhiman, *Phys. Rev. C* **74**(3), 034323 (2006)
- [47] V. Thakur, R. Kumar, P. Kumar *et al.*, *Phys. Rev. C* **106**, 045806 (2022)
- [48] T. B rvenich, D. Madland, and P. G. Reinhard, *Nucl. Phys. A* **744**, 92 (2004)
- [49] S. Kirkpatrick, *Journal of Statistical Physics* **34**, 975 (1984)
- [50] J. Dobaczewski, W. Nazarewicz, and P. Reinhard, *J. Phys. G: Nucl. Part. Phys.* **41**, 074001 (2014)
- [51] C. Mondal, B. Agrawal, and J. De, *Phys. Rev. C* **92**, 024302 (2015)
- [52] M. Kumar, S. Kumar, V. Thakur *et al.*, *Phys. Rev. C* **107**(5), 055801 (2023)
- [53] W. C. Chen and J. Piekarewicz, *Phys. Lett. B* **748**, 284 (2015)
- [54] S. Brandt, *Statistical and computational methods in data analysis* (Springer, 1997)
- [55] P. G. Reinhard and W. Nazarewicz, *Phys. Rev. C* **81**, 051303 (2010)
- [56] H. de Vries, C. W. de Jager, and C. de Vries, *Atom. Data Nucl. Data Table* **36**, 495 (1987)
- [57] M. Wang, G. Audi, F. Kondev *et al.*, *Chin. Phys. C* **41**, 030003 (2017)
- [58] I. Angeli and K. P. Marinova, *At. Data Nucl. Data Tables* **99**, 69 (2013)
- [59] A. Sharma, M. Kumar, S. Kumar *et al.*, *Nucl. Phys. A* **1040**, 122762 (2023)
- [60] C. Pruitt, R. Charity, L. Sobotka *et al.*, *Phys. Rev. Lett.* **125**, 102501 (2020)
- [61] J. Birkhan, M. Miorelli, S. Bacca *et al.*, *Phys. Rev. Lett.* **118**(25), 252501 (2017)
- [62] A. Tamii *et al.*, *Phys. Rev. Lett.* **107**(6), 062502 (2011)
- [63] C. M. Tarbert *et al.* (Crystal Ball at MAMI and A2 Collaboration), *Phys. Rev. Lett.* **112**(24), 242502 (2014)
- [64] J. Piekarewicz, *AIP Conf. Proc.* **1128**, 144 (2009)
- [65] J. Jastrzebski, A. Trzcinska, P. Lubiski *et al.*, *Int. J. Mod. Phys. E* **13**, 343 (2004)
- [66] W. G. Newton and G. Crocombe, *Phys. Rev. C* **103**(6), 064323 (2021)
- [67] J. Xu and P. Papakonstantinou, *Phys. Rev. C* **105**(4), 044305 (2022)
- [68] H. Gil, P. Papakonstantinou, and C H. Hyun, *Int. J. Mod. Phys. E* **31**, 2250013 (2022)
- [69] Y. Li, H. Chen, D. Wen *et al.*, *Eur. Phys. J. A* **57**, 1 (2021)
- [70] J. M. Lattimer, *Particles* **6**, 30 (2023)
- [71] G. Colo, U. Garg, and H. Sagawa, *Eur. Phys. J. A* **50**, 26 (2014)
- [72] J. Piekarewicz, *Eur. Phys. J. A* **50**, 25 (2014)
- [73] M. Tsang, Y. Zhang, P. Danielewicz *et al.*, *Phys. Rev. Lett.* **102**, 122701 (2009)
- [74] P. Danielewicz and J. Lee, *Nucl. Phys. A* **922**, 1 (2014)
- [75] J. R. Oppenheimer and G. M. Volkoff, *Phys. Rev.* **55**, 374 (1939)
- [76] R. C. Tolman, *Phys. Rev.* **55**, 364 (1939)
- [77] G. Baym, C. Pethick, and P. Sutherland, *Astrophys. J.* **170**, 299 (1971)
- [78] E. Fonseca, T. T. Pennucci, J. A. Ellis *et al.*, *Astrophys. J.* **832**, 167 (2016)
- [79] E. Annala, T. Gorda, A. Kurkela *et al.*, *Phys. Rev. Lett.* **120**(17), 172703 (2018)
- [80] R. Abbott *et al.*, *Astrophys. J. Lett.* **896**, L44 (2020)
- [81] T. Hinderer, *Astrophys. J.* **677**, 1216 (2008)
- [82] T. Hinderer, *Astrophys. J.* **697**, 964 (2009)
- [83] T. Hinderer, B. D. Lackey, R. N. Lang *et al.*, *Phys. Rev. D* **81**, 123016 (2010)